JCTC Journal of Chemical Theory and Computation

pubs.acs.org/JCTC Article

Activity-Induced Droplet Inversion in Multicomponent Liquid–Liquid Phase Separation

Published as part of Journal of Chemical Theory and Computation special issue "Developments of Theoretical and Computational Chemistry Methods in Asia".

Xianyun Jiang and Zhonghuai Hou*

Cite This: https://doi.org/10.1021/acs.jctc.5c00162 Read Online

ACCESS | Metrics & More | Article Recommendations | Supporting Information

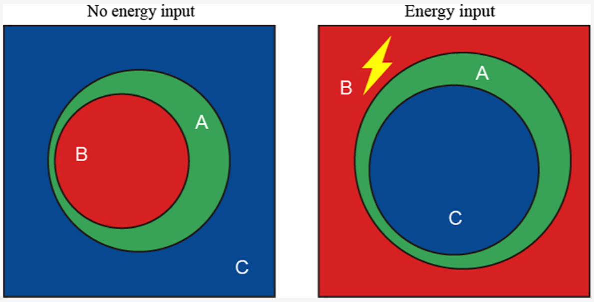

ABSTRACT: Liquid–liquid phase separation (LLPS) is a vital process in forming membrane-free organelles, crucial for cell physiology and recently gaining significant attention. However, the effects of nonequilibrium factors, which are common in real life, on the process of LLPS have not been fully explored. To address this issue, we developed a model for nonequilibrium phase separation involving three components (A, B, and C) by integrating a nonequilibrium term into the chemical potential for active component B. We find significant changes in the morphology and dynamics of nonequilibrium phase-separated droplets compared to their equilibrium counterparts. Remarkably, with a large enough activity, the B-A-C structure (B at the center, surrounded by A, then enveloped by C) under equilibrium conditions may change to a C-A-B structure. Further simulations give a global picture of the system under both active and passive conditions, revealing the shifts of the phase boundaries and unraveling the effect of activity on different droplet structures. We derived an effective free energy for the active LLPS system to provide a qualitative understanding of our observations. Our study presents a basic model for nonequilibrium phase separation processes, providing crucial insights into LLPS alongside intracellular nonequilibrium phenomena.

1. INTRODUCTION

Liquid–liquid phase separation (LLPS), as an underlying mechanism for the formation of biomolecular condensates,[1] has received much attention in recent years. The important role of LLPS in cell physiology and disease has become increasingly apparent.[2,3] Growing evidence indicates LLPS plays a key role in the normal function of cells, such as the regulation of gene expression,[4] signal transduction,[5] and cellular stress responses.[6] Notably, the process of LLPS has been demonstrated to modulate the spatial distribution of biomolecules within the intracellular environment. This, in turn, has been shown to affect the biological functions of these biomolecules.[7,8] For example, the demixing HSP70 and TDP43 ensure the anisosome generation and thus prevent TDP-43 aggregation,[7] and multilayered liquids of proteins facilitate sequential RNA processing reactions in RNP bodies.[8] Theoretical understanding of such structure formation has also received attention. Based on equilibrium thermodynamics, phase behavior,[9] and morphology control[10] of such a system have been proposed.

However, there are a large number of nonequilibrium factors in the cell, such as energy input from hydrolysis of ATP,[11] maintenance of concentration gradients,[6] and nonequilibrium chemical reactions.[12,13] While most studies focus on the phase separation process at equilibrium,[1,14,15] some researchers have explored these nonequilibrium factors. For example, Jülicher et al. find that nonequilibrium chemical reactions can control the LLPS droplets of pericentriolar material.[16] The phenomenon of splitting of droplet[17] and formation of spherical shell[18] are also found in LLPS involved with nonequilibrium chemical reactions. For the energy input by ATP hydrolysis, it is reported that active components, which utilize energy input in the cell to perform directional motions, can control the LLPS system.[19−21] Microtubular-based active fluid is reported to suppress LLPS of DNA nanostars,[20] and motor protein Myosin 1D on the branched actin network can control the droplet formations of p62 bodies.[21] These results reveal a possible mechanism of spatiotemporal regulation of LLPS through active matter in cells, emphasizing the importance of understanding the impact of active matter on LLPS. However, theoretical studies of LLPS processes involving active

Received: January 28, 2025
Revised: March 17, 2025
Accepted: March 18, 2025

ACS Publications

components, especially for multicomponent LLPS, are still lacking.

To address this issue, in this article, we construct a three-component LLPS model with one active component. To describe the nonequilibrium characteristics of active matter, active field theory provides a means by incorporating nonequilibrium terms.[22,23] Based on this, we introduce a minimal nonequilibrium term to chemical potential in our model. Then, we perform phase-field simulations to show the influences of activity on the evolution of phase-separated droplets, in which we found new droplet structures and shifts of boundary lines. To qualitatively understand these results, we derive an effective free energy to analyze the influence of the active component.

The sections of this paper are as follows. Section 2 provides an overview of the model used to simulate the active LLPS. Section 3 explores the dynamics of the system over a range of interaction parameters. The comparative presentation and discussion of phase diagrams in nonequilibrium and equilibrium states are also provided herein. Finally, the conclusions of the paper can be found in Section 4.

2. MODEL

We start from a three-component system (A, B, and C) with the equilibrium free energy F_0 given by the Flory–Huggins theory,[24,25] as described below

$$F_0 = \int \left(\frac{\varepsilon^2}{2} \left[\sum_i |\nabla \phi_i|^2 \right] + \sum_i \phi_i \ln \phi_i + \sum_{i \neq j} \chi_{ij} \phi_i \phi_j \right) \mathrm{d}V \tag{1}$$

$$\mu_i^{\,0} = \frac{\delta F_0}{\delta \phi_i} \tag{2}$$

$$\dot{\phi}_i = \nabla \cdot (M_i \nabla \mu_i^{\,0}) \tag{3}$$

where ϕ_i is the volume fraction of each component i and μ_i^0 is corresponding chemical potential. The first term of F_0 is the Cahn–Hilliard gradient penalty term with typical interface width ε, which ensures droplet formation. Entropy contribution from mixing and enthalpy from intermolecular interaction are termed $\phi_i \ln \phi_i$ and $\chi_{ij}\phi_i\phi_j$, respectively. χ_{ij} regulates the strength of the interactions between each pair of components, and larger χ_{ij} means larger repulsion between component i and j. After constructing an expression for the chemical potential μ^0, we can calculate the evolution of volume fraction ϕ_i by model B dynamics, representing in eq 3, in which M_i is the mobility of each component. By adjusting the value of interaction parameters χ_{AB}, χ_{BC}, and χ_{AC} (white bars in Figure 1), we can obtain many types of equilibrium structures,[7,10] including the common bilayer structure in cell,[7] as illustrated in Figure 1.

To address the effects of active matter, active field theory[22,23] can be used to examine the directional motion of active matter with energy inputs. From the study of active field theory, these nonequilibrium properties are reflected by introducing a series of active terms, which are primarily manifested in higher-order gradient terms that are not able to be represented in equilibrium free energy F_0, thus breaking time-reversal symmetry in an equilibrium system.[26] These active terms reflect the nonequilibrium characteristics brought about by the directional movement of active particles, thereby enabling the realization of special phenomena observed in active particle simulations.[22,23] Specifically, introducing an active term in chemical potential level (Active Model B) results in uncommon tangent construction of dense and dilute phase,[22] and a more complex model (Active Model B+) introduces nonequilibrium terms at the current level, resulting in microphase separation and reverse Ostwald ripening.[23] In this work, we focus on the active term at the chemical potential level, as shown in the following equation

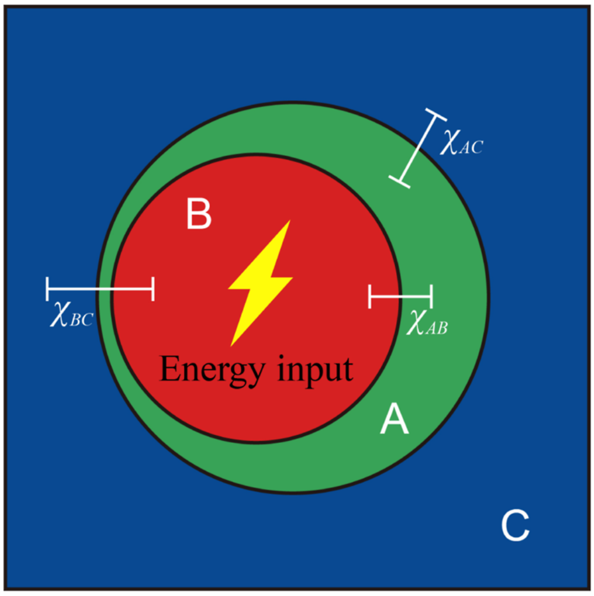

Figure 1. Illustration of the active LLPS model. Three components A, B, and C, are represented in red, green, and blue colors, respectively. Component B is the active component with energy input. The white bars represent the interaction coefficients χ, where the length indicates the strength magnitude.

$$\mu_i = \mu_i^{\,0} + \lambda_i |\nabla \phi_i|^2 \tag{4}$$

The λ_i in term $\lambda_i|\nabla\phi_i|^2$, controls how far from equilibrium the component is. The component i is under equilibrium when $\lambda_i = 0$, and becomes active with $\lambda_i \neq 0$. The dynamics of ϕ_i, as proposed by Active Model B,[22] can also be expressed in the form of model B dynamics with μ^0 replaced by μ

$$\dot{\phi}_i = \nabla \cdot (M_i \nabla \mu_i) \tag{5}$$

For numerical simulations of the above equations, the length of the simulation box in two dimensions was set as a unit length and divided into a 128 × 128 grid with periodical boundary conditions for spatial discretization. A semi implicit time-integration method was used for time discretization. To improve numerical stability, the Fourier spectrum method[10] was used. Detailed simulation methods are shown in the Supporting Information. For parameters used in simulation, the volume fraction of three components is fixed as $\phi_A/\phi_B/\phi_C = 0.1{:}0.3{:}0.6$. For simplicity, the mobility coefficients are set equal for each component, i.e., $M_i = M = 1.0$, and the penalty factor for concentration gradients ε is fixed to 10^{-4}. In the subsequent sections, we focus on the scenario where only component B exhibits activity ($\lambda_B \neq 0$, while $\lambda_A = \lambda_C = 0$) and omit the subscript "B" in λ_B for brevity. Regarding the interaction parameters among the components, we adopted a fixed value of $\chi_{AB} = 2.5$ for simplicity. Other parameters will be provided in each specific simulation setup as detailed in the following sections. For the initial state of the simulation, we use a small fluctuation (5%) around uniform distributions.

3. RESULTS

3.1. Typical Phenomena. To start, inspired by the typical bilayer structure in cells,[7,8] we consider the parameter $\chi_{AC} = 3.0$ and $\chi_{BC} = 5.0$ for the formation of such a structure. The snapshots of the equilibrium system, in which the dense phases of A, B, and C are colored green, red, and blue, respectively, are shown in Figure 2a. In the initial stage ($t = 10.0$), there are several small droplets, followed by coarsening progress over time ($t = 200.0$) to form a large droplet finally ($t = 1000.0$). As shown in the last row of Figure 2a, the system displays a bilayer structure, characterized by a ring of component A surrounding component B and an external layer of component C.

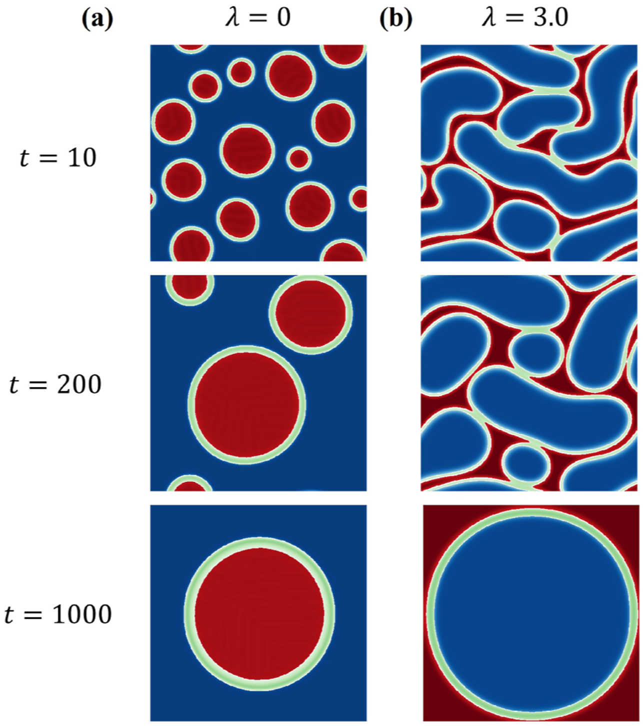

Figure 2. Snapshot of system under $\chi_{AC} = 3.0$ and $\chi_{BC} = 5.0$ for $t = 10.0$, $t = 200.0$, and $t = 1000.0$ in passive state ($\lambda = 0$) for (a) and active state ($\lambda = 3.0$) for (b).

The simulation results of the active case $\lambda > 0$ are shown in Figure 2b. Interestingly, although we still observe bilayer structures in the system at $t = 10.0$, the spatial distribution of each component is significantly different compared to the passive state, with C located inside the ring of A and B located outside. We refer to this configuration as an inverted droplet in the latter. Coarsening persists in the active system, and at $t = 1000.0$, a large droplet with a bilayer structure is formed, in which the distribution of components B and C is still inverted compared to the passive state. Due to the importance of droplets in realizing their biological functions, these results suggest that activity may serve as a means of structural regulation to control the switch of specific functions of LLPS droplets. Supporting Information, Videos S2 shows the morphological transformation of the droplet as component B becomes active, providing a possible example of this regulation.

The appearance of inverted droplets illustrates the existence of a strong influence of activity on the droplet structure in the LLPS system. To study the influence of activity on typical structures under equilibrium, we simulate a series of parameters. For simplicity, we first fixed the two parameters $\chi_{AB} = 2.5$ and $\chi_{AC} = 3.0$ and gradually increased χ_{BC} from $\chi_{BC} = 2.0$. Snapshots of the equilibrium system are shown in Figure 3a. With increasing χ_{BC}, the system transitioned from a homogeneous state (single-phase) to the state with mixed phase-separated droplets by A and B (two-phase) and then to the formation of a bilayer structure (three-phase). As a comparison, the droplet morphology in the active state is shown in Figure 3b, in which single-phase, two-phase, and three-phase structures also emerge when χ_{BC} increase. For $\chi_{BC} = 2.0$ and 2.5, there is not much difference between the passive and active ones. However, as shown in the third column of Figure 3, the active system already shows a three-phase structure when $\chi_{BC} = 3.0$, while the equilibrium one remains in the two-phase region. Meanwhile, the shapes of A and B are

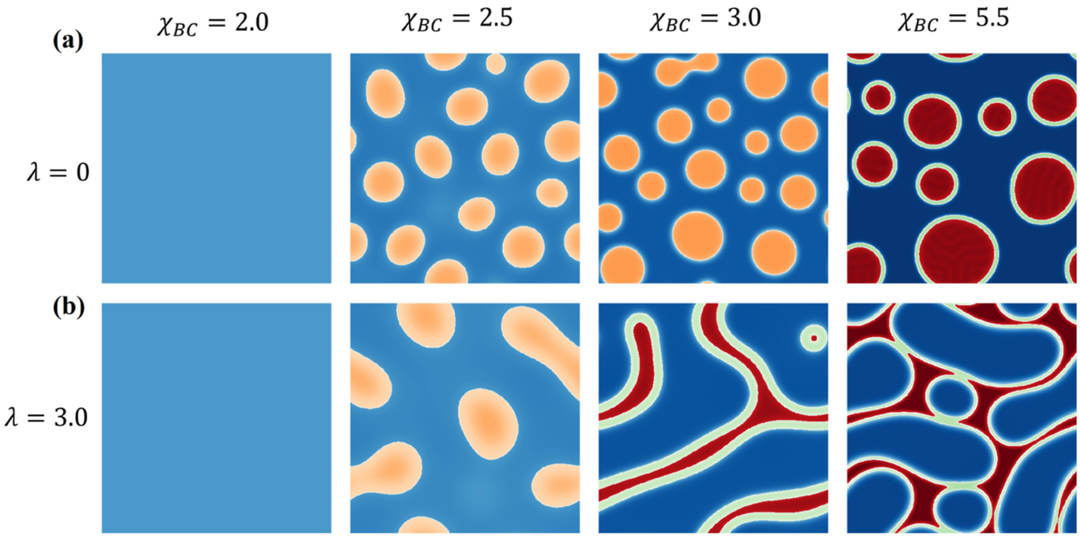

Figure 3. Snapshot of the system in passive (a) and active (b) state at different χ_{BC} parameters and fixed $\chi_{AC} = 3.0$ at $t = 10.0$. The phase colored orange represents a mixed A and B phases.

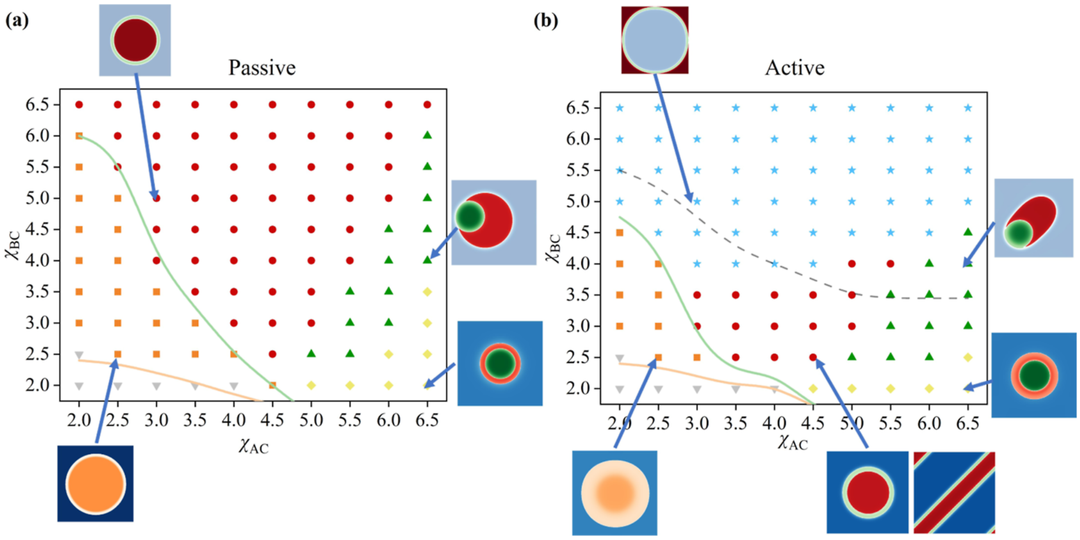

Figure 4. Phase diagram of system in χ_{AC}−χ_{BC} parameter space, passive state λ = 0 for (a), and active state λ = 3.0 for (b). Solid lines represent phase region boundaries obtained from theoretical analyses. Snapshots of the steady states under corresponding parameters are depicted around the phase diagram.

also different, forming a striped structure. Furthermore, when χ_{BC} = 5.5, the droplet structure is inverted in the active system, like the case in Figure 2. Comparison of Figure 3a,b reveals not only a significant transformation in the morphology of the nonequilibrium droplets but also differences in the number of coexisting phases in the system. These observations highlight the significant impact of active matter on LLPS.

3.2. Phase Diagrams. To have a global picture of the system state under various parameters, we plotted the phase diagrams of the system in parameter space χ_{AC} and χ_{BC} for the passive state (Figure 4a) and active state (Figure 4b). We identified dense phases for each substance based on a volume fraction threshold (typically ϕ^{crit} = 0.7). The overall system state was then determined based on the structural relationships between these dense phases and labeled accordingly using distinct symbols (see Figure S1 for examples). We first take a look at the passive case. When χ_{AC} and χ_{BC} are both small, only a homogeneous state exists (denoted by gray triangles). With a moderate χ_{AC} (χ_{AC} = 3.0, for example), as χ_{BC} increases, the system exhibits a transition from a single-phase to two-phase and then three-phase state. With even larger χ_{AC}, only three-phase regions exist. In the three-phase region, with different settings of χ_{AC} and χ_{BC}, there are three typical structures, ring formed by A (red square), ring formed by B (yellow square), and crescent structure (green triangle).

Subsequently, by comparing the phase diagrams of active and nonactive systems, significant changes occurred in the system morphology. For the state denoted by red squares, both sphere and striped structures may emerge in the late stage under active conditions. For the crescent structure denoted by green triangles, the shape of the droplets deviates from a sphere and is elongated into an ellipse. The biggest difference in the active case is that the inverted droplet, in which C is located inside of the ring by A and B located outside, emerges for all χ_{AC} when χ_{BC} is large. This structure, absent under equilibrium conditions across all χ_{AC}−χ_{BC} parameter spaces, highlights the distinctive effects of active matter. Besides the morphology changes, the overall distribution of single-phase, two-phase, and three-phase zones in the phase diagram also changes. We can see that the areas of the region denoted by orange spheres are significantly smaller compared to the passive case. Thus, we conclude that the boundaries of each region are also shifted, which means that the critical value of χ_{BC} for transition in the number of coexisting phases is different compared to the passive case.

In summary, from the comparison between passive and active states, the effects of activity are a distortion of the droplet morphology and shifts in boundaries. The most interesting phenomenon is the inversion droplet formation when χ_{BC} is large. Noting that in the active field theory of MIPS, the binodal of phase separation is shifted with active parameter λ,[26] and the shift of critical lines in our system may also be attributed to the effects of the activity. To this end, further analyses are proposed following to understand these findings.[5]

3.3. Theoretical Analysis. We start by considering the shifts in the boundaries. It is widely known that the number of coexisting phases in the system depends on the structure of the potential energy surface, such as the common tangent construction in a two-component phase-separation system. Considering the equilibrium case, we calculate the number of coexisting phases in each set of parameters by the convex hull method.[9,27] Specifically, we apply the convex hull method on the bulk free energy density $f = \sum_i \phi_i \ln \phi_i + \sum_{i\neq j}\chi_{ij}\phi_i\phi_j$ concerning the different volume fractions of A, B, and C under each parameter set χ_{ij}, and we determine the number of coexisting phases at the point of ϕ_i in this work. Details of such construction are listed in Supporting Information. After determining the number of coexisting phases for all parameters, the boundaries of each region can be obtained, which are shown by the solid line in Figure 4a. We can see the boundary matches very well with the distribution of structures obtained by the simulation. To acquire the boundaries for active cases, we need to construct an effective free energy to perform equilibrium-like analyses to obtain the thermodynamic properties of the system. As proposed in active field theory,[22] to reflect the contribution of activity gradient terms, pseudodensity, effective free energy, and pseudopressure can be used to play the roles of volume fraction, free energy, and pressure under equilibrium conditions. In our system, we use a

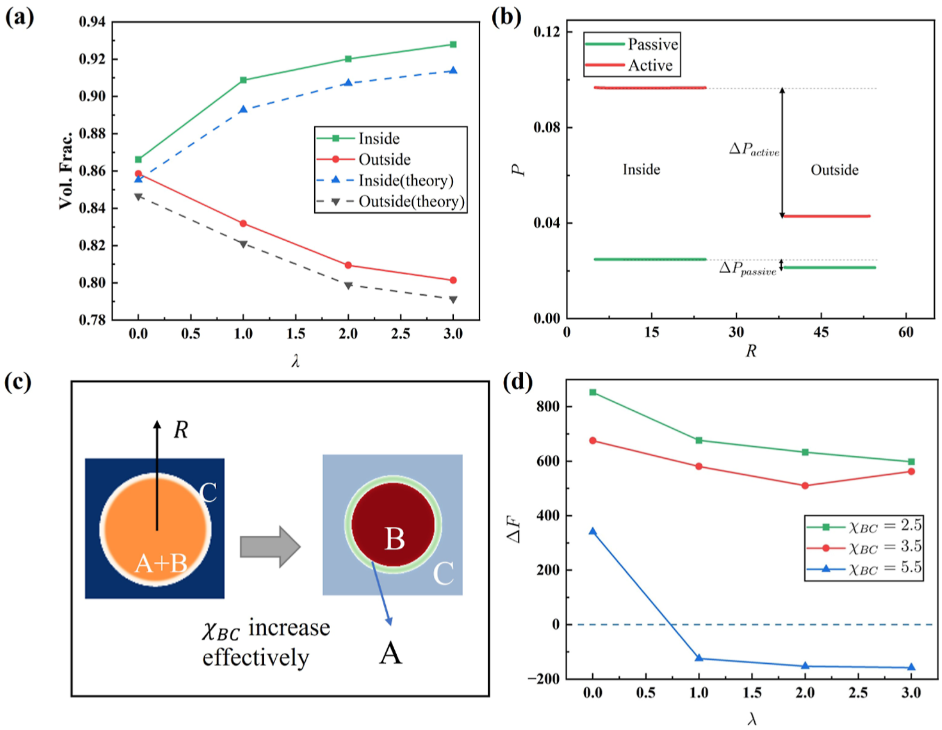

Figure 5. Theoretical analyses of active LLPS system. (a) The volume fraction of major components inside (component B) and outside (component C) of the droplet in theory (solid line) and simulation (dashed line) varies with activity under the parameter $\chi_{AC} = 3.0$ and $\chi_{BC} = 3.5$. (b) Pseudopressure and pressure difference between inner and outer droplets in active and passive states. (c) Illustration of activity-induced transformation of two-phase structure into three-phase structure. (d) Effective free energy difference of original and inverted droplet varies with activity with $\chi_{AC} = 3.0$.

mapping from the volume fraction of the active component ϕ_B to pseudodensity ψ_B and the bulk free energy f to effective free energy g, as shown in the following equations

$$\frac{\partial^2\psi_B}{\partial\phi_B^2} = -\frac{2\lambda}{\varepsilon^2}\frac{\partial\psi_B}{\partial\phi_B}$$

$$\frac{\partial g}{\partial\phi_A} = \frac{\partial f}{\partial\phi_A} = \mu_A$$

$$\frac{\partial g}{\partial\psi_B} = \frac{\partial f}{\partial\phi_B} = \mu_B. \tag{6}$$

The specific expression of g is given in Supporting Information, due to its complexity. Likewise, we can determine the transition line between one-, two-, and three-phase regions from g, as shown in solid lines in Figure 4b, which matches well with the regions obtained from the simulation. By a comparison of the differences in transition lines between active and inactive states, it is evident that a transition occurs in the active system at a lower χ_{BC} value. This implies that activity may influence the effective interactions within the system. Subsequently, we endeavor to understand this behavior from this perspective.

Considering that interactions can influence the composition of phases within a system, we calculate the dense phase volume fraction of each component by both simulation (solid line) and theory (dashed line) under the parameters $\chi_{AC} = 3.0$ and $\chi_{BC} = 3.5$, as shown in Figure 5a. We find that the volume fraction of B (inside the droplet) is larger with a larger activity, and the volume fraction of C (outside the droplet) declines. These changes can correspond to an increase in χ_{BC} in the equilibrium system. Furthermore, as the components of the sphere droplet are determined by the combination of pressure difference inside and outside the sphere, which can be written as $P(\phi_{\text{out}}) = P(\phi_{in}) + \sigma/R$, in which σ represents surface tension, we can calculate the pressure by $P = \phi_A\mu_A + \psi_B(\phi_B)\mu_B - g(\phi_A, \psi_B)$ and get the pressure difference in both active ($\lambda = 3.0$) and passive cases using the volume fraction calculated by simulation, as shown in Figure 5b. The enlarged pressure difference origins from the activity of B, demonstrating a bigger effective surface tension σ in the active case and again proving the effective increase in χ_{BC}, regarding that surface tension is related to the interaction parameter χ.[10] We conclude that increased activity enhances effective interactions, resulting in different droplet structures. Figure 5c illustrates the transition behavior from two phases to three phases with increasing effective interaction parameters, χ_{BC} in the active case.

Finally, we turn to the emergence of the inverted droplet state. We conducted calculations to compare the total effective free energies of original and inverted droplets, as illustrated in the final row of Figure 2, under different λ and χ_{BC}. The difference in total energy ΔF between the inverted and original droplet is visualized in Figure 5d. For small χ_{BC}, a positive free energy difference indicates that the energy of the original droplet is lower, and inverted droplets become energetically favorable when the χ_{BC} is significantly large. The dashed line in Figure 4b illustrates the critical χ_{BC} for droplet inversion at various χ_{AC}, which elucidates the spontaneous occurrence of droplet inversion under conditions of high χ_{BC}. Increased χ_{BC} leads to a higher volume fraction of B in the dense phase, indicating that a sufficiently high concentration of active substance B is a prerequisite for inverted droplet formation.

4. DISCUSSION

In this study, we maintained a fixed volume fraction ratio for each component at $\phi_A/\phi_B/\phi_C$ = 0.1:0.3:0.6. With different ratios, such as $\phi_A/\phi_B/\phi_C$ = 0.2:0.2:0.6, we observed that inverted droplets did not form under the parameters leading to droplet inversion in the previous sections ($\chi_{AC} = 3.0$, $\chi_{BC} = 6.0$, and $\chi_{AB} = 2.5$). When the ratio of B was increased to 0.15:0.25:0.6, inverted droplets appeared again, as shown in Figure S4, showing a sufficient quantity of active substance B is necessary for the formation of inverted droplets. Furthermore, simulations revealed the absence of inverted droplets when $\lambda < 0.5$ across all parameters χ_{AC}−χ_{BC} used in Figure 4, indicating a certain threshold level of activity to induce inversion. Through our analysis, we infer that the intriguing phenomenon of droplet inversion occurs when the activity and the volume fraction of active component B in its dense phase are large enough. For theoretical analyses, we try to use effective free energy to understand the phenomena of active LLPS systems; however, not all the results are discussed here. For example, the causes of nonsphere droplets are still unclear, which remain to be studied in further work.

In summary, we developed a three-component model of phase separation with an active component to investigate the influence of active matter on the LLPS. A notable discovery was the activity-induced inversion of the droplet interiors and exteriors under specific conditions. Through extensive simulations, we systematically examined the impact of the active component on various structures, highlighting shifts in the phase boundary within the phase diagram and morphology changes in each droplet structure. To understand these phenomena, we derived expressions for the effective free energy. These expressions enabled the calculation of phase boundaries and the identification of energetically favorable structures in the active LLPS system.

The spatial arrangement of biological components is crucial for their physiological functions. Regulating this distribution through energy-driven active components may be important for the formation of membrane-free structures in organisms. Many cellular processes involve active participation and the creation of nonequilibrium states. While droplet inversion has not been observed in current experimental systems, nonspherical shapes similar to those in our study have been detected in previous research,[20,28] highlighting the potential of controlling the morphology of LLPS by active components. In intracellular contexts, nonequilibrium processes often entail the interplay of various agents like actin, kinesin, and the cytoskeleton, fueled by energy from ATP hydrolysis. LLPS may involve complex interactions between multiple active components, and further investigation is needed to analyze such scenarios. Considering the complexity of such systems, more refined phase field models are needed, such as introducing the detailed properties of biomolecules such as chain length, charge distribution, etc. It is also very important to establish the connection between the real nonequilibrium processes and the activity terms, e.g., by deriving the nonequilibrium terms from the real intracellular transport process. To this end, more complex active field theory, including active terms in the current level in active model B+[29] or introducing active nematic,[20] may play a role. Besides theoretical analyses, active substances in biological systems can also be studied experimentally both in vitro and in vivo. Examples include in vitro motility assays[30] and single-molecule fluorescence microscopy for probing human myosin.[31] These techniques hold promise for investigating active phase separation systems. Integrating theoretical and experimental approaches will enhance our understanding of nonequilibrium LLPS processes in real-life systems.

■ ASSOCIATED CONTENT

Supporting Information

The Supporting Information is available free of charge at https://pubs.acs.org/doi/10.1021/acs.jctc.5c00162.

Detailed simulation methods, formula derivation, and additional simulation snapshots (PDF)

Evolution of system with parameter $\lambda = 3.0$, $\chi_{AC} = 3.0$, and $\chi_{BC} = 5$ (MP4)

Evolution of system with parameter $\chi_{AC} = 3.0$ and $\chi_{BC} = 5.0$ (MP4)

■ AUTHOR INFORMATION

Corresponding Author

Zhonghuai Hou − *Department of Chemical Physics, Hefei National Research Center for Physical Sciences at the Microscale, University of Science and Technology of China, Hefei, Anhui 230026, China*; orcid.org/0000-0003-1241-7041; Email: hzhlj@ustc.edu.cn

Author

Xianyun Jiang − *Department of Chemical Physics, Hefei National Research Center for Physical Sciences at the Microscale, University of Science and Technology of China, Hefei, Anhui 230026, China*; orcid.org/0009-0001-6725-1926

Complete contact information is available at: https://pubs.acs.org/10.1021/acs.jctc.5c00162

Notes

The authors declare no competing financial interest.

■ ACKNOWLEDGMENTS

This work is supported by MOST-NSFC(2022YFA1303100 and 32090040) and the Strategic Priority Research Program of the Chinese Academy of Sciences (XDB0450402).

■ REFERENCES

(1) Hyman, A. A.; Weber, C. A.; Jülicher, F. Liquid-liquid phase separation in biology. *Annu. Rev. Cell Dev. Biol.* **2014**, *30*, 39−58.

(2) Shin, Y.; Brangwynne, C. P. Liquid phase condensation in cell physiology and disease. *Science* **2017**, 357, No. eaaf4382.

(3) Banani, S. F.; Lee, H. O.; Hyman, A. A.; Rosen, M. K. Biomolecular condensates: organizers of cellular biochemistry. *Nat. Rev. Mol. Cell Biol.* **2017**, *18*, 285−298.

(4) Boisvert, F.-M.; Van Koningsbruggen, S.; Navascués, J.; Lamond, A. I. The multifunctional nucleolus. *Nat. Rev. Mol. Cell Biol.* **2007**, *8*, 574−585.

(5) Li, P.; Banjade, S.; Cheng, H.-C.; Kim, S.; Chen, B.; Guo, L.; Llaguno, M.; Hollingsworth, J. V.; King, D. S.; Banani, S. F.; et al. Phase transitions in the assembly of multivalent signalling proteins. *Nature* **2012**, *483*, 336−340.

(6) Brangwynne, C. P.; Eckmann, C. R.; Courson, D. S.; Rybarska, A.; Hoege, C.; Gharakhani, J.; Jülicher, F.; Hyman, A. A. Germline P granules are liquid droplets that localize by controlled dissolution/condensation. *Science* **2009**, *324*, 1729−1732.

(7) Yu, H.; Lu, S.; Gasior, K.; Singh, D.; Vazquez-Sanchez, S.; Tapia, O.; Toprani, D.; Beccari, M. S.; Yates, J. R., III; Da Cruz, S.; et al.

HSP70 chaperones RNA-free TDP-43 into anisotropic intranuclear liquid spherical shells. *Science* **2021**, *371*, No. eabb4309.

(8) Feric, M.; Vaidya, N.; Harmon, T. S.; Mitrea, D. M.; Zhu, L.; Richardson, T. M.; Kriwacki, R. W.; Pappu, R. V.; Brangwynne, C. P. Coexisting liquid phases underlie nucleolar subcompartments. *Cell* **2016**, *165*, 1686−1697.

(9) Mao, S.; Kuldinow, D.; Haataja, M. P.; Košmrlj, A. Phase behavior and morphology of multicomponent liquid mixtures. *Soft Matter* **2019**, *15*, 1297−1311.

(10) Mao, S.; Chakraverti-Wuerthwein, M. S.; Gaudio, H.; Košmrlj, A. Designing the morphology of separated phases in multicomponent liquid mixtures. *Phys. Rev. Lett.* **2020**, *125*, 218003.

(11) Kanematsu, Y.; Narita, A.; Oda, T.; Koike, R.; Ota, M.; Takano, Y.; Moritsugu, K.; Fujiwara, I.; Tanaka, K.; Komatsu, H. Structures and mechanisms of actin ATP hydrolysis. *Proc. Natl. Acad. Sci. U.S.A.* **2022**, *119*, No. e2122641119.

(12) Strulson, C. A.; Molden, R. C.; Keating, C. D.; Bevilacqua, P. C. RNA catalysis through compartmentalization. *Nat. Chem.* **2012**, *4*, 941−946.

(13) Söding, J.; Zwicker, D.; Sohrabi-Jahromi, S.; Boehning, M.; Kirschbaum, J. Mechanisms for active regulation of biomolecular condensates. *Trends Cell Biol.* **2020**, *30*, 4−14.

(14) Ren, Q.; Li, L.; Liu, L.; Li, J.; Shi, C.; Sun, Y.; Yao, X.; Hou, Z.; Xiang, S. The molecular mechanism of temperature-dependent phase separation of Heat shock factor 1. *Nat. Chem. Biol.* **2025**.

(15) Li, L.; Hou, Z. Crosslink-Induced Conformation Change of Intrinsically Disordered Proteins Have a Nontrivial Effect on Phase Separation Dynamics and Thermodynamics. *J. Phys. Chem. B* **2023**, *127*, 5018−5026.

(16) Zwicker, D.; Decker, M.; Jaensch, S.; Hyman, A. A.; Jülicher, F. Centrosomes are autocatalytic droplets of pericentriolar material organized by centrioles. *Proc. Natl. Acad. Sci. U.S.A.* **2014**, *111*, E2636−E2645.

(17) Zwicker, D.; Seyboldt, R.; Weber, C. A.; Hyman, A. A.; Jülicher, F. Growth and division of active droplets provides a model for protocells. *Nat. Phys.* **2017**, *13*, 408−413.

(18) Bergmann, A. M.; Bauermann, J.; Bartolucci, G.; Donau, C.; Stasi, M.; Holtmannspötter, A. L.; Jülicher, F.; Weber, C. A.; Boekhoven, J. Liquid spherical shells are a non-equilibrium steady state of active droplets. *Nat. Commun.* **2023**, *14*, 6552.

(19) Caballero, F.; Marchetti, M. C. Activity-suppressed phase separation. *Phys. Rev. Lett.* **2022**, *129*, 268002.

(20) Tayar, A. M.; Caballero, F.; Anderberg, T.; Saleh, O. A.; Cristina Marchetti, M.; Dogic, Z. Controlling liquid−liquid phase behaviour with an active fluid. *Nat. Mater.* **2023**, *22*, 1401−1408.

(21) Feng, X.; Du, W.; Ding, M.; Zhao, W.; Xirefu, X.; Ma, M.; Zhuang, Y.; Fu, X.; Shen, J.; Zhang, J.; et al. Myosin 1D and the branched actin network control the condensation of p62 bodies. *Cell Research* **2022**, *32*, 659−669.

(22) Wittkowski, R.; Tiribocchi, A.; Stenhammar, J.; Allen, R. J.; Marenduzzo, D.; Cates, M. E. Scalar φ 4 field theory for active-particle phase separation. *Nat. Commun.* **2014**, *5*, 4351.

(23) Solon, A. P.; Stenhammar, J.; Cates, M. E.; Kafri, Y.; Tailleur, J. Generalized thermodynamics of phase equilibria in scalar active matter. *Phys. Rev. E* **2018**, *97*, 020602.

(24) Flory, P. J. Thermodynamics of High Polymer Solutions. *J. Chem. Phys.* **1942**, *10*, 51−61.

(25) Huggins, M. L. Solutions of Long Chain Compounds. *J. Chem. Phys.* **1941**, *9*, 440.

(26) Nardini, C.; Fodor, E.´.; Tjhung, E.; Van Wijland, F.; Tailleur, J.; Cates, M. E. Entropy production in field theories without time-reversal symmetry: quantifying the non-equilibrium character of active matter. *Phys. Rev. X* **2017**, *7*, 021007.

(27) Lin, Y.-H.; Brady, J. P.; Forman-Kay, J. D.; Chan, H. S. Charge pattern matching as a ‘fuzzy’mode of molecular recognition for the functional phase separations of intrinsically disordered proteins. *New J. Phys.* **2017**, *19*, 115003.

(28) Spoelstra, W. K.; Van Der Sluis, E. O.; Dogterom, M.; Reese, L. Nonspherical coacervate shapes in an enzyme-driven active system. *Langmuir* **2020**, *36*, 1956−1964.

(29) Tjhung, E.; Nardini, C.; Cates, M. E. Cluster phases and bubbly phase separation in active fluids: reversal of the Ostwald process. *Phys. Rev. X* **2018**, *8*, 031080.

(30) Warshaw, D. M. The in vitro motility assay: a window into the myosin molecular motor. *Physiology* **1996**, *11*, 1−7.

(31) Berg, A.; Velayuthan, L. P.; Tågerud, S.; Ušaj, M.; Månsson, A. Probing actin-activated ATP turnover kinetics of human cardiac myosin II by single molecule fluorescence. *Cytoskeleton* **2024**, *81*, 883−901.